Transition control using a single plasma actuator

R. Joussot*

Laboratoire PRISME, Université d'Orléans,
8, rue Léonard de Vinci,
45072, Orléans, Cedex 2, France
and
GREMI UMR 6606,
CNRS – Université d'Orléans,
14 rue d'Issoudun, 45067, Orléans Cedex 2, France
E-mail: romain.joussot@univ-orleans.fr
*Corresponding author

R. Weber and A. Leroy

Laboratoire PRISME, Université d'Orléans,
8, rue Léonard de Vinci,
45072, Orléans, Cedex 2, France
E-mail: regine.weber@univ-orleans.fr
E-mail: annie.leroy@univ-orleans.fr

D. Hong

GREMI UMR 6606,
CNRS – Université d'Orléans,
14 rue d'Issoudun, 45067, Orléans Cedex 2, France
E-mail: dunpin.hong@univ-orleans.fr

Abstract: The aim of this study is to modify, by using surface plasma actuators, the laminar-to-turbulent transition location of a Blasius boundary layer developing on a flat plate mounted in an opened wind tunnel. Measurements of flow velocities were performed by hot wire anemometry. Results show that an actuator placed upstream the natural transition zone enables the promotion or the delay of the transition onset, depending on the location, the voltage amplitude, and the frequency of the high voltage electrical parameters.

Keywords: surface DBD; plasma actuator; transition; laminar boundary layer.

Reference to this paper should be made as follows: Joussot, R., Weber, R., Leroy, A. and Hong, D. (2013) 'Transition control using a single plasma actuator', *Int. J. Aerodynamics*, Vol. 3, Nos. 1/2/3, pp.26–46.

Biographical notes: R. Joussot obtained his PhD in Gas and Plasma Physics from the University of Orléans in 2010. He worked in the plasma laboratory GREMI (C.N.R.S. and University of Orléans) on study and development of plasma actuators, in order to use these devices for active flow control.

R. Weber is an Assistant Professor at the Polytechnique Engineer School of University of Orléans since 2001. She is a Researcher at PRISME Laboratory inside ESA 'Écoulements et Systèmes Aérodynamiques' team. Her research deals with active flow control by plasma actuators, and consists of the characterisation of the actuators and their effects on a flow.

A. Leroy is an Assistant Professor in Fluids Mechanics at IUT of Orléans since 1999. She is a Researcher at PRISME Laboratory inside ESA 'Écoulements et Systèmes Aérodynamiques' team. Her research deals with wind tunnel experiments dedicated to refine physical understanding and characterisation of flows, in view of active flow control, more particularly with plasma actuators.

D. Hong is a Professor at University of Orléans and works in the plasma laboratory GREMI of C.N.R.S. and the University of Orléans. He received his PhD in Plasma Spectroscopy from the University of Orléans. Since several years, he has involved in a collaborative project concerning the use of electrical discharge as actuator dedicated to subsonic airflow control.

1 Introduction

Plasma actuators have been used for several years to modify flows around a wide range of geometries. Most of these results are reviewed by Moreau (2007) and Corke et al. (2009). The main goal of the majority of these studies is to improve the aerodynamic characteristics of the studied geometries by drag reduction and/or lift enhancement. They can be achieved by modifying the location of the laminar-to-turbulent transition of the natural boundary layer. Transition delay can induce a reduction of skin-friction drag and transition advancement can increase stall incidences by promoting a turbulent boundary layer more resistive to large positive pressure gradient occurring around airfoil leading edge for example.

The transition occurs according to several forcing disturbances in the environment as surface roughness or free stream turbulence for example. Two main scenarios can be distinguished in transition onset in which free stream turbulence is a key parameter. At a low free stream turbulence level (below 0.2%), the *classical* (or *natural*) scenario is effective. Natural instabilities occur inside the laminar boundary layer. These instabilities are first, two-dimensional Tollmien-Schlichting waves (Schubauer and Skramstad, 1948; Schlichting, 1979), which then turn into secondary instabilities (Herbert, 1988), leading to the transition onset. If the secondary instabilities take the shape of single or double 'spikes' inside the laminar boundary layer (Klebanoff et al., 1962), the transition scenario is named *K*-type transition. The spikes multiply, leading to the formation of turbulent spots (Emmons, 1951). A good review of the *K*-type transition can be found in Kachanov (1994). For a higher free stream turbulence level (above 0.5% to 1%), perturbations of the external flow induce three-dimensional instabilities inside the boundary layer, triggering the transition which is named *bypass* transition. An overview of the numerous pathways by which the laminar boundary layer becomes turbulent is given by Saric et al. (2002).

Surface DBD plasma actuators producing a mean 2D wall jet have been successfully applied to transition control over a flat plate geometry. The actuators generally consist of two metallic electrodes separated by a dielectric material. One electrode is connected to a high voltage power supply, while the second one is grounded, thereby creating an intense electric field at the surface of the actuator. The surrounding air is then ionised and a non-thermal plasma is created in which the charged species drift along the electric field and collide with the neutral species. Momentum is thus transferred from these ionised species to the air, inducing a flow of a few m.s^{-1} called 'ionic wind'. The ionic wind is created at the actuator frequency, and has the properties of a wall-jet: its maximum is close to the wall near the plasma region and it diffuses downstream.

The ability of such actuators to modify a boundary layer has been clearly demonstrated by numerous studies. In Séraudie et al. (2006), Porter et al. (2007) and Magnier et al. (2009), the laminar-to-turbulent transition is promoted because plasma actuators induce an increase in the mean and fluctuation streamwise velocities just downstream the actuator. Other authors have shown that it is also possible to delay transition using plasma actuators producing a stabilising effect on the velocity profiles. In works of Grundmann and Tropea (2007, 2009), Boucinha et al. (2008) and Séraudie (2008), plasma actuators induce a higher level of fluctuation velocity downstream the actuators. However, this higher level of fluctuation of velocity remains constant downstream whereas previously it increases without control up to the onset of transition. In Grundmann and Tropea (2008, 2009), plasma actuators are used on a boundary layer where 2D perturbations are artificially generated. These disturbances could be similar to TS-waves and are induced at a particular frequency of 55 Hz. By acting in a pulsed mode (on-off) at the same frequency, plasma actuators damp these fluctuations. This damping of artificial TS-waves is clearly illustrated on the energy spectra reported by the authors.

Numerical investigations on transition modification by plasma actuators had also been performed. Quadros (2009) calibrated a model of the body force produced by a plasma actuator in quiescent air from experimental measurements (PIV). This semi-empirical model was used to simulate the ionic wind effects in the near wall region of actuator. LES of a flat plate showed that it was possible to delay the transition with a continuous action, inducing a drag reduction of around 20%. Moreover, Quadros (2009) demonstrated that TS-waves could be cancelled by an anti-phase sinusoidal modulation of the body force. He showed in particular that the amplitude of the TS-waves was damped of about 90%, leading to a delay of the transition. Duchmann et al. (2009) highlighted the ability of plasma actuators to manipulate the boundary layer profiles since the linear stability analysis showed that the boundary layer was stabilised with actuator ON. The authors concluded that the stabilising effect of the plasma actuator is an important factor in transition manipulation, and that the wave damping is an additional and effective effect which can be superimposed to the stabilising one.

The objective of the present study is to find out the respective conditions for which a single plasma actuator can either delay or promote the natural transition of a flat plate boundary layer. Several parameters were tested in order to demonstrate their influence on the transition onset: actuator position, voltage amplitude, and working frequency.

2 Experimental details

2.1 Plasma actuator setup

The plasma actuator consists of two metallic electrodes separated by a dielectric material. The electrodes are made of adhesive copper foil tape with a thickness of 86 μm (including the adhesive). The dielectric panel is composed of three layers of two dielectric materials. A 500 µm thick Mylar sheet is set between two Kapton sheets (55 µm thick). Thus, the overall thickness is about 610 µm. The multi-layer disposition of the dielectric panel was chosen to ensure a good resistance to the dielectric breakdown with a thickness as thin as possible. The electrodes are asymmetrically positioned on the two sides of the dielectric panel as shown on Figure 1. A 3 mm gap is set between the upper and lower electrodes. For the actuator configuration presented here, this gap prevents the untimely appearance of the filamentary regime as mentioned by Forte et al. (2006). Both electrodes are 150 mm in length and 6 mm in width. The electrodes have rounded tips and are placed in an asymmetrical arrangement in the spanwise direction. The tips of the upper electrode are shifted by 20 mm relative to those of the lower electrode, as shown on Figure 1. Rounded shifted tips are used here to prevent spark ignition. Several Kapton layers are placed below the actuator in order to inhibit plasma formation on this side. Encapsulation does not affect ionic wind generation on the upper side, as checked by Laurentie et al. (2009). The upper electrode is connected to an AC power supply. This actuator setup has been previously characterised in Boucinha et al. (2008).

In the present setup, the running actuator operates in steady mode for driving voltages (V_{HV}) ranging from 8 to 12.7 kV and frequencies (f_{HV}) ranging from 250 to 1,500 Hz. The electrical consumption for such electrical parameters is approximately ranging from 1.6 to 6.7 W. A high voltage probe (Tektronix Series P6015A, 75 MHz, 3.0 pF) is used to measure the voltage applied to the actuator. A Rogowski-type current probe (Bergoz CT 1.0) is used to measure the discharge current through the actuator. Voltage and current signals are monitored on a digital oscilloscope (LeCroy WaveSurfer Series, 64 Xs-A, 600 MHz, 2.5 Gs/s, 8 bits).

Figure 1 Schematic of a single plasma actuator, (a) side view and (b) top view (see online version for colours)

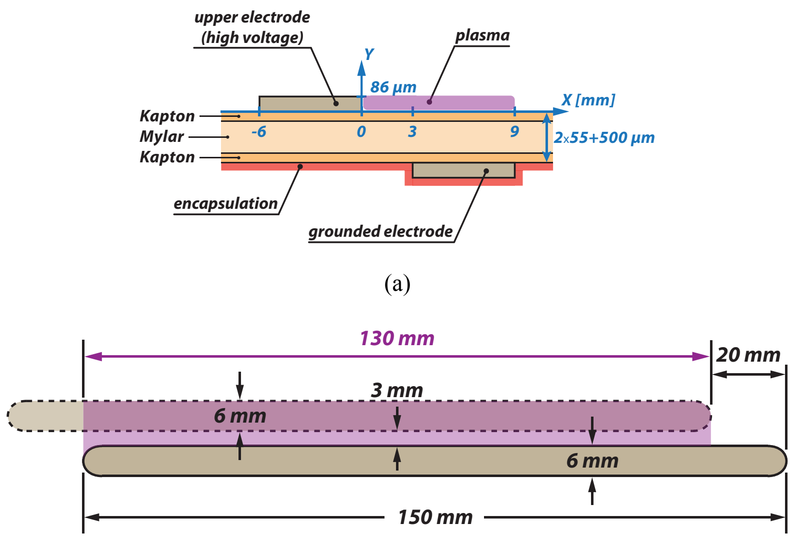

(b)

2.2 *Wind tunnel and flat plate*

The 30 mm thick flat plate is placed horizontally inside the test section of an open wind tunnel with a 16:1 contraction ratio. The working section is 50 cm × 50 cm and 2 m long. The plate is mounted at 50% of the test section height between two lateral vertical plates made of see-through PMMA (each 2 cm thick). The vertical plates have sharp leading edges in order to prevent flow disturbances near the flat plate surface. The flat plate does not span the entire width of the test section but only 60%, and is therefore 30 cm in width. A schematic of the flat plate mounted inside the test section is shown in Figure 2.

The flat plate is composed of several parts made of dielectric material. The 60 mm long leading edge of the plate consists of the first 30% chord length of a NACA 0015 profile. The actuator insert is placed thanks to two lateral mounts, each 84 cm long. The actuator insert is made of a 20 cm wide and 1 m long acrylic plate. Single plasma actuators can be mounted on its surface depending on experimental requirements. The surface on the insert where no actuators will be mounted is covered with a dielectric panel (the same materials as for the actuator). The flat plate trailing edge consists of the 30% to 100% chord length NACA 0015 profile (140 mm long). The trailing edge angle is not adjustable and is set at 0° as for the leading edge. In order to consider the leading edge curvature, the curvilinear abscissa (s) is used herein.

Figure 2 Schematic of the flat plate, (a) side view and (b) top view (see online version for colours)

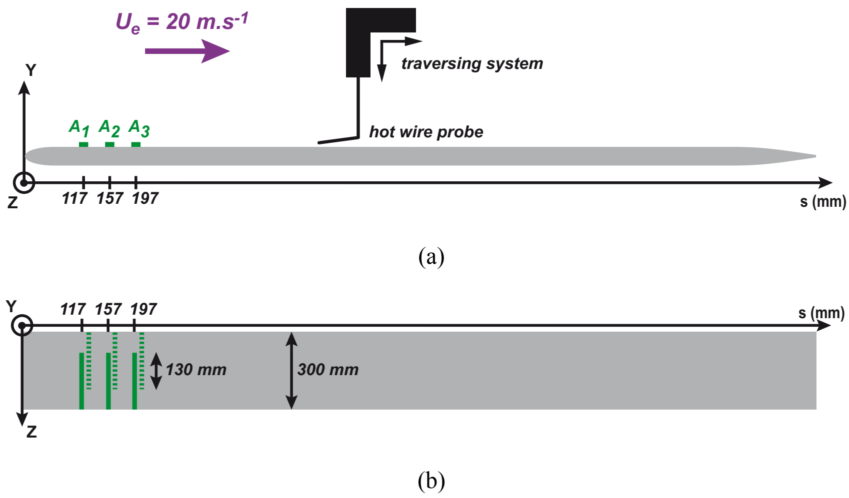

In this study, three single plasma actuators are mounted on the plate (A_1, A_2 and A_3). The first one is placed at s_{A1} = 117 mm, the second at s_{A2} = 157 mm and the third at s_{A3} = 197 mm. These positions correspond to the end of the upper electrode where the plasma begins to spread over the actuator surface. The electrical connections are independent of each other and non-intrusive with respect to the boundary layer development over the flat plate surface. As the actuators are fired one by one, the non-working upper electrodes are removed in order to minimise disturbances on the boundary layer. The removed electrodes can be easily put back in place.

2.3 Hot wire measurements

Measurements of the flow velocity are made using a one-dimensional hot-wire probe (Dantec Dynamics, 55P15). The longitudinal component of the velocity is measured in this study. The probe is calibrated from 0.5 to 35 m.s^{-1} using a Dantec calibration unit. The hot-wire signal is recorded with a National Instruments A-D data acquisition card connected to a PC. The software used to perform these measurements is StreamWare. Each velocity measurement consists of the average of 327,680 samples, sampled at 30 kHz (acquisition frequency of 60 kHz low-pass filtered). The velocity measurement duration for each point is therefore about 11 s. A temperature correction is applied to the hot-wire data.

The probe is mounted on a moving three-axis traversing system (Isel Automation LF5 Series). The resolution step of each axis is 0.1 mm with a precision of 0.02 mm on each position. The hot-wire position close to the wall is determined with a webcam (Logitech QuickCam Pro 9000) associated to a spyglass. A test pattern of graph paper is placed just ahead of the probe and the optical device is pointed at the hot-wire prongs. By visualising the prongs' reflection on the wall, the hot-wire position can be precisely determined. This mirrored image technique is presented more fully in the review by Örlü et al. (2010). The uncertainty of the wall location versus the hot wire is found to be within ±0.1 mm.

It was checked the high voltage did not induce strong perturbations onto the hot-wire signal. The velocity signal was studied for a position 40 mm downstream the actuator A_2, which was fired. Fluctuations generated by the DBD appeared on the velocity signal. Two mean velocities were calculated from the signal, one with the perturbations and one without (the 1 kHz activity due to the DBD was removed numerically). It was concluded these fluctuations did not induce differences on the calculated velocities since the error was less than 1%.

3 Baseline flows

In this section, the natural and the non-manipulated boundary layers are studied in order to confirm what the type of transition is, and to check that the active electrode does not affect the boundary layer development. The boundary layer was first mapped with no upper electrodes mounted. This is the natural flow case. This case was then compared with non-manipulated cases which correspond to an upper electrode mounted (A_1, A_2 or A_3) on the flat plate with the actuator non-running.

3.1 The natural flow

The free stream velocity was set at 20 m.s^{-1} in order to have the transition regime downstream the actuators and near the middle of the flat plate. First of all, the mean velocity variation comparing to the free stream velocity of the first measurement point was plotted (Figure 3). Measurements were taken at a constant height y = 80 mm. An increase of a few percent in the mean velocity was noted and is relative to a favourable pressure gradient of –20 Pa.m^{-1}. No peak level of mean velocity is observable above the leading edge (s < 80 mm) because of the height of the measurement points. Turbulence intensity (Tu) is defined as $Tu = u_{rms} / U_e$ and is about 0.26% along the flat plate. This turbulence level is quite low and indicates that transition may be of the *natural* type, not *bypass*.

Figure 3 Relative mean velocity fluctuation (+) and turbulence intensity (open symbol) along the flat plate at y = 80 mm (see online version for colours)

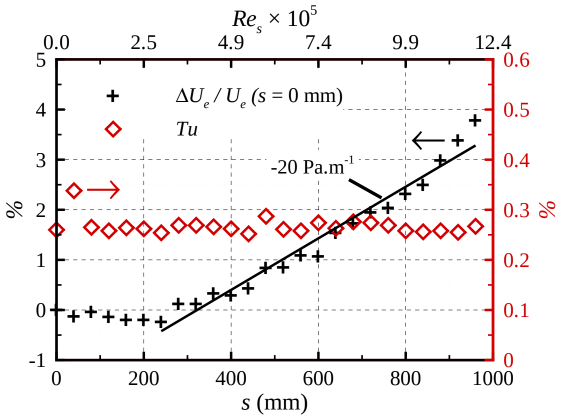

The boundary layer was mapped by performing velocity profiles at different longitudinal positions. Each profile consists of velocity measurements of 30, 40 or 50 wall-normal positions (along the y-axis). The number of measurement points depends on the boundary layer thickness. In order to check the distance between the surface and the first y-position, a linear interpolation of the near-wall part of the profile was performed. This technique allows to check whether the hot-wire is affected by heat conduction of the wall. Free stream velocity U_e was determined outside the boundary layer for each s-axis position. The boundary layer thickness δ_{99} is defined as the height from the wall where velocity corresponds to 99% of U_e.

Figure 4 Mean velocity profiles at different longitudinal positions, (a) $Re_s = 1.5 \times 10^5$ to 4.9×10^5 and (b) $Re_s = 5.4 \times 10^5$ to 8.9×10^5 (see online version for colours)

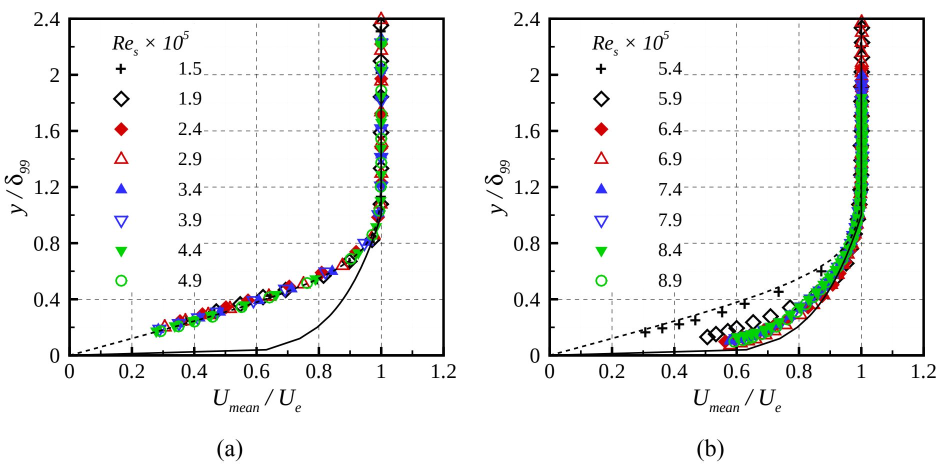

Note: Dashed lines are Blasius profiles and solid lines are Prandtl profiles.

Figure 4 shows mean velocity profiles for the natural flow along the flat plate. The boundary layer is clearly laminar for the first positions since the mean velocity profiles are superimposed on the theoretical Blasius curve. Downstream velocity profiles begin to deviate from the Blasius solution to tend towards the Prandtl profile. The boundary layer is transitional and then becomes fully turbulent. Transition occurs downstream position s = 437 mm where $Re_s = 5.4 \times 10^5$, which is consistent with the range defined by Schlichting (1979).

Figure 5 Velocity fluctuation profiles at different longitudinal positions, (a) $Re_s = 1.5 \times 10^5$ to 4.9×10^5 and (b) $Re_s = 5.4 \times 10^5$ to 8.9×10^5 (see online version for colours)

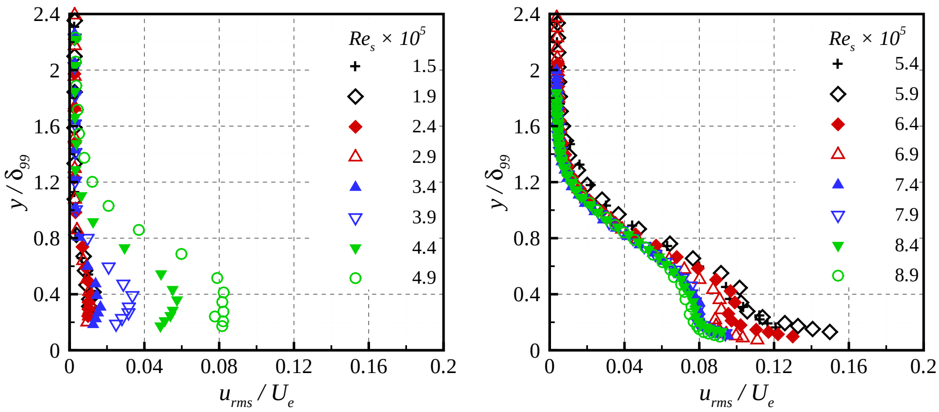

(a) (b)

In order to have more information into the nature of the transition, velocity fluctuations u_{rms} were studied at several downstream positions. Figure 5(a) shows profiles of u_{rms} for the laminar boundary layer. The maximum level of u_{rms} / U_e is constant and about 1.3% for the first four positions. For the next positions, the velocity fluctuations start to grow with a maximum remaining at the same height (y / δ_{99} = 0.4). This continuous growth of u_{rms} means the onset of the transition. Figure 5(b) shows u_{rms} profiles for the second part of the flat plate. Whereas previously the shape of u_{rms} profiles exhibited only one maximum, a second one now appears close to the wall. This near-wall maximum is due to the turbulence motion inside the boundary layer, indicating the onset of turbulence (Arnal and Juillen, 1978). In this study, the downstream variation of velocity fluctuation profiles is similar to that reported in Schubauer and Klebanoff (1956).

Streamwise distributions of the maximum value of u_{rms} / U_e found across the boundary layer, and u_{rms} / U_e at a constant wall-normal position of y / δ_{99} = 0.4 are reported in Figure 6. The shapes of the curves are similar and exhibit three main parts. In the first one, velocity fluctuations are weak. Then the laminar flow breaks down and the transition region begins. As u_{rms} grows, the near-wall maximum appears, explaining why the two curves deviate from each other. Velocity fluctuations at y / δ_{99} = 0.4 reach a peak level above 10% of the free stream velocity where the boundary layer is transitional, typically reported in Klebanoff et al. (1962). Then u_{rms} levels decrease slightly until they reach a plateau where the flow is fully turbulent. This particular shape of the u_{rms} streamwise distribution is classical (Fransson et al., 2006) and relative to the K-type transition scenario (Kachanov, 1994).

Figure 6 Velocity fluctuation distribution along the flat plate at a constant non-dimensional height of $y / \delta_{99} = 0.4$ (+) and at variable height where u_{rms} / U_e is maximal to a given longitudinal position (open symbol)

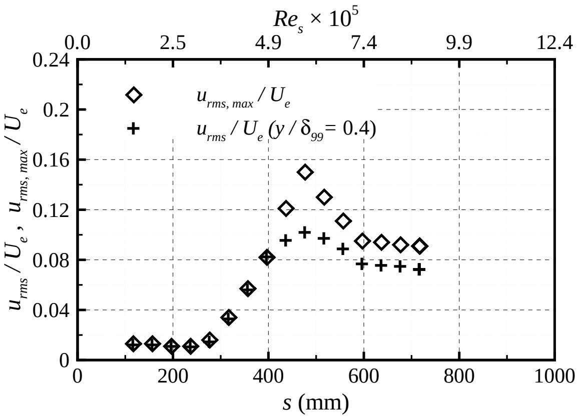

Figure 7 (a) Power spectral density of velocity fluctuation and (b) instantaneous velocity signal inside the boundary layer and just above it, at s-position s = 117 mm ($Re_s = 1.5 \times 10^5$) (see online version for colours)

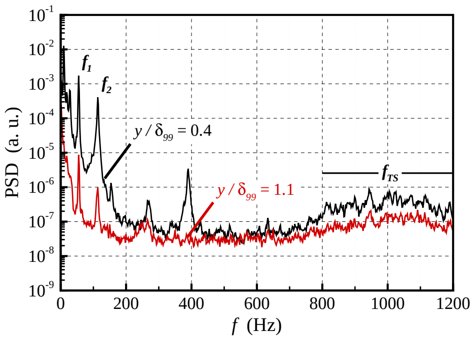

(a)

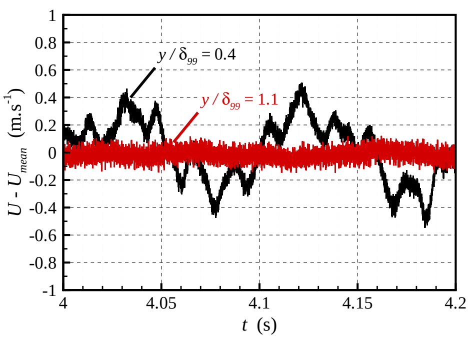

(b)

In the laminar part of the boundary layer, the low level of velocity fluctuations means that TS-waves are present inside the boundary layer. Indeed a maximum fluctuation level of about 1% is ordinarily associated with the fact that two-dimensional TS-waves exist and are going to shortly turn into three-dimensional secondary instabilities (Herbert, 1988). The energy spectra of u_{rms} [Figure 7(a)] show a frequency activity around 1 kHz. This activity could be associated with TS-waves. Indeed, u_{rms} profiles filtered on the frequency band 800–1,200 Hz show the distinctive shape of a u_{rms} profile of a boundary layer in which TS-waves are present (Figure 8). The detection of TS-waves is difficult due to the turbulence intensity level which is about 0.3%: this value may be considered as a detection threshold for TS-waves (Kendall, 1990). This explains why the bi-modal shape of the u_{rms} profile with the typical footprint of TS-waves (Schlichting, 1979) is not visible on Figure 5(a), but only on Figure 8. The spectrum inside the boundary layer is dominated by low-frequency contributions [f_1 and f_2 on Figure 7(a)] which are not TS-waves (Arnal et al., 1977). These low-frequency motions are due to the response of the boundary layer to external disturbances in the free stream flow. These contributions are clearly visible on the instantaneous velocity for a wall-normal position inside the boundary layer, which shows a low-frequency oscillation [Figure 7(b)]. Amplitude of TS-waves is weak in comparison to the overall fluctuation level.

Figure 8 Contribution of the velocity fluctuations in the frequency band 800–1,200 Hz for the positions above actuator A_1 (s_{A1} = 117 mm, $Re_s = 1.5 \times 10^5$), actuator A_2 (s_{A2} = 157 mm, $Re_s = 1.9 \times 10^5$), and actuator A_3 (s_{A3} = 197 mm, $Re_s = 2.4 \times 10^5$) (see online version for colours)

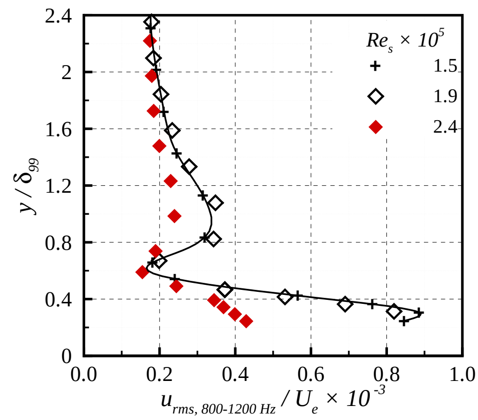

In the second part of the boundary layer, u_{rms} begins to grow and the instantaneous velocity profiles exhibit single and double spikes (Figure 9). These spikes are responsible for the final laminar boundary layer breakdown and the onset of transition (Klebanoff et al., 1962). They correspond to the three-dimensional secondary instabilities induced by unstable TS-waves. Spikes are more and more present in the velocity signals until turbulent spots appear (at s = 397 mm, i.e., $Re_s = 4.9 \times 10^5$), leading to a fully turbulent boundary layer.

Figure 9 Instantaneous velocity signal near the middle of the boundary layer (y / δ_{99} = 0.4) at an s-position where spikes appear (u_{rms} / U_e = 4%, s = 317 mm, i.e., $Re_s = 3.9 \times 10^5$)

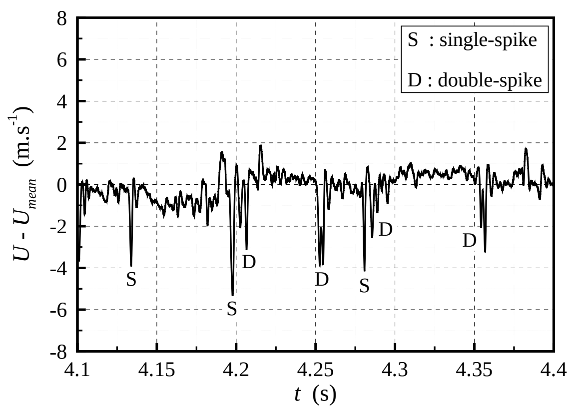

Figure 10 Streamwise distribution of (a) the boundary layer thickness δ_{99} and (b) the shape factor H_{12} (see online version for colours)

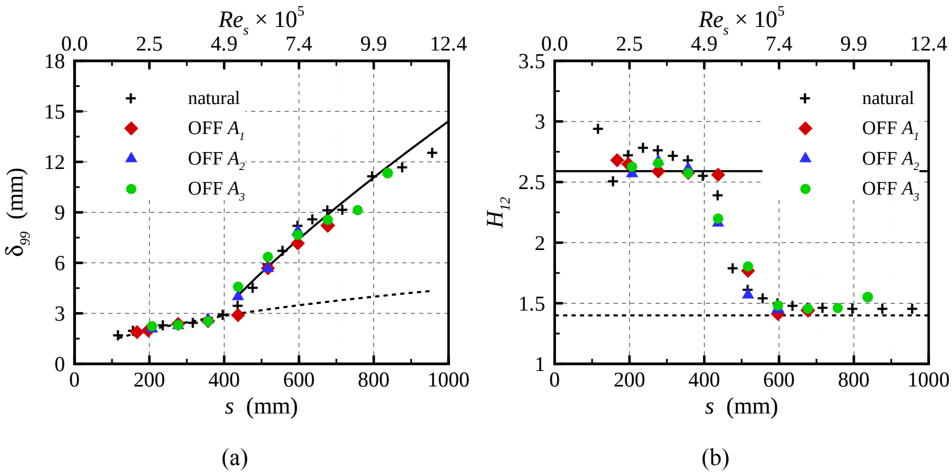

Note: Natural flow without electrode mounted (+) and non-manipulated cases with upper electrode of actuators A_1 (diamond), A_2 (delta) and A_3 (circle) are reported.

3.2 *The non-manipulated flow*

In order to act on the transition position, one upper electrode has to be mounted on the flat plate surface corresponding to the active plasma actuator (A_1, A_2 or A_3). It must therefore be ensured that this electrode does not induce any disturbances on the boundary layer development. The non-intrusivity of the electrode was checked by studying the streamwise distributions of the boundary layer thickness and shape factor H_{12} (Figure 10). They were compared to those of the natural boundary layer (i.e., without an upper electrode mounted). The data show that the position of transition is slightly affected by the high-voltage electrode. From now on, the boundary layer development along the flat plat is considered the same whatever the case: natural or non-manipulated. Thus the natural case (without electrode) is taken as the baseline flow in order to compare the actuators.

4 Acting on transition: two approaches

The present section discusses the results obtained on transition control using plasma actuators. Two approaches were considered, depending on which parameter was constant. Firstly, action position and high voltage amplitude were changed with a constant frequency of f_{HV} = 1 kHz. Then, a plasma actuator was selected in order to determine the sensitivity of transition to the actuator frequency f_{HV}. In this case, the ionic wind velocity was maintained constant by adjusting the high voltage amplitude V_{HV} for each frequency tested.

Figure 11 Shape factor (H_{12}) distribution along the flat plate for the cases where transition is (a) promoted, (b) delayed, and (c) not changed (see online version for colours)

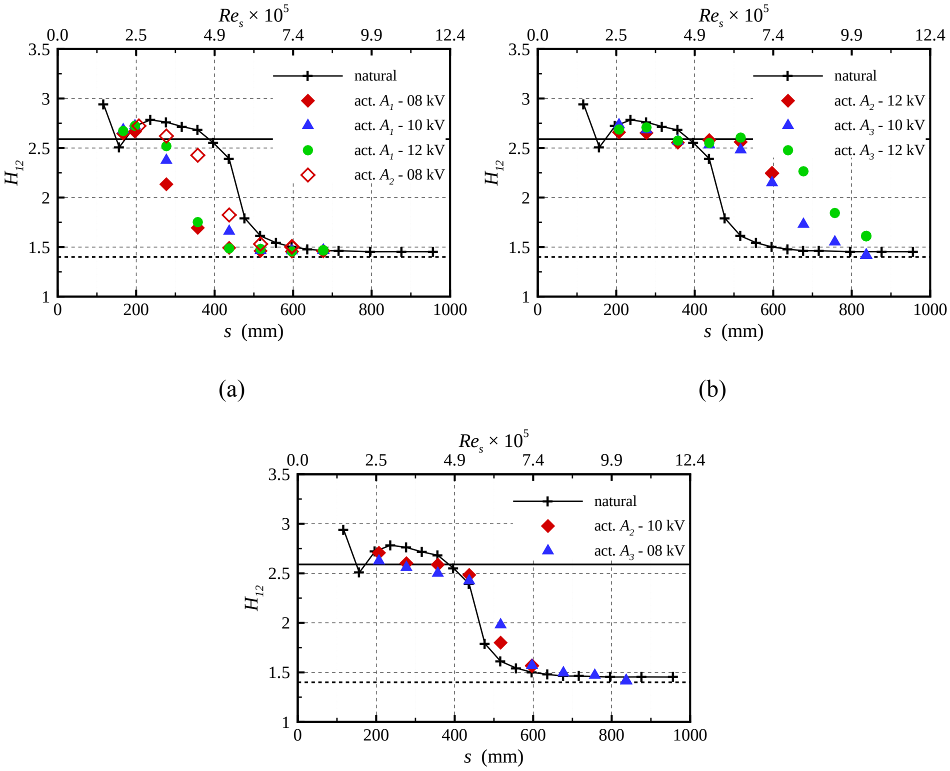

(a) (b)

(c)

4.1 Parametric study: voltage amplitude and action position

The parametric study is dedicated to studying the influence of the action position and voltage amplitude. The following parameters were used: s_{A1} = 117 mm, s_{A2} = 157 mm and s_{A3} = 197 mm for the position; and V_{HV} = 8, 10 and 12 kV for the amplitude. Depending on these parameters, the plasma actuator does not have the same effect on the transition position. It is possible to delay the transition position [Figure 11(a)], to promote it [Figure 11(b)] and even to leave it unchanged [Figure 11(c)]. The effect of the ionic wind on the boundary layer development was determined using the shape factor H_{12}. Actuators A_1 and A_2 allow to promote the transition. For actuator A_2, only the lowest amplitude induces a promotion of transition. For the actuator A_3, the greatest voltage amplitude induces the highest transition delay. It is also reported here that actuators A_2 and A_3 seem to produce the same effect on the boundary layer transition for different voltage amplitudes.

The effects of plasma actuators on the transition position are summarised in Table 1. In the top row, the maximum velocity of the ionic wind U_{act}^* is reported under the voltage amplitude. It corresponds to the ionic wind velocity at the end of the plasma area just over the dielectric surface (Boucinha et al., 2011). This velocity can be estimated using the following empirical law: $U_{act}^* = \alpha f_{HV}(V_{HV} - V_0) + \beta(V_{HV} - V_0)$, where $\alpha = 0.17$ m.kV^{-1} and $\beta = 0.38$ m.kV^{-1}.s^{-1} are two constants, f_{HV} is the actuator frequency in kHz, and $V_0 = 4$ kV is the ignition voltage of the actuator. This law was proposed by Boucinha (2009) with the same actuator design. The three actuators induce different effects on the transition even when they are driven with the same voltage amplitude (e.g., for $V_{HV} = 10$ kV). Thus, it is not only the ionic wind velocity which is important here but the shape of the boundary layer where the momentum is added in the flow (i.e., the position of the actuator). In addition, when the actuator A_2 is selected, it is possible to obtain the three effects on the transition position, for three different ionic wind velocities. In this particular case, the boundary layer shape is the same, meaning that it is the momentum added in the flow that is important.

Table 1 Summary of plasma actuator effects on the transition position

	$V_{HV} = 8$ kV $U_{act}^* = 2.2$ m.s^{-1}	$V_{HV} = 10$ kV $U_{act}^* = 3.3$ m.s^{-1}	$V_{HV} = 12$ kV $U_{act}^* = 4.4$ m.s^{-1}
Actuator A_1	Promoting	Promoting	Promoting
$s_{A1} = 117$ mm, $Re_s = 1.5 \times 10^5$	–170 mm	–170 mm	–130 mm
Actuator A_2	Promoting	No effect	Delaying
$s_{A2} = 157$ mm, $Re_s = 1.9 \times 10^5$	–110 mm	+20 mm	+140 mm
Actuator A_3	No effect	Delaying	Delaying
$s_{A3} = 197$ mm, $Re_s = 2.4 \times 10^5$	+30 mm	+140 mm	+240 mm

Note: The number under the effect (promoting, no effect, delaying) indicates change in the transition position ($f_{HV} = 1$ kHz)

In summary, for a given frequency (here $f_{HV} = 1$ kHz), the effect of the ionic wind on the transition depends on the momentum, and the place where it is added. The effect of the plasma actuator on the transition can be summed up as follows. First, the closer the actuator is to the transition point, the greater the transition delay, for a given amplitude voltage. Second, the greater the ionic wind velocity is, the greater the transition delay, at a given action position.

In order to determine what is changed inside the boundary layer when the actuator is fired, the velocity fluctuation distributions were studied (Figure 12). For a given voltage amplitude of $V_{HV} = 10$ kV, the three effects are shown. An early increase of u_{rms} means that the transition onset is promoted; this is the case for actuator A_1. Indeed, from the first measurement point, the u_{rms} / U_e level is greater than in the natural flow. Then, it increases until reaching its maximum level and tends to a plateau. This distribution has a similar pattern as the natural flow except that it occurs earlier. In this case, the plasma actuator seems to excite the boundary layer sufficiently to trigger the transition onset. For the neutral case, the manipulated and natural boundary layers have almost the same u_{rms} distributions. Transitional and turbulent parts are close but for the part where the boundary layer is laminar, the u_{rms} / U_e levels are higher than those in the natural case. Thus, the boundary layer is excited downstream the actuator, but not enough to shift the position of the transition.

Figure 12 Velocity fluctuation distributions along the flat plate at a constant non-dimensional height (y / δ_{99} = 0.4) for the natural and manipulated boundary layers (V_{HV} = 10 kV) (see online version for colours)

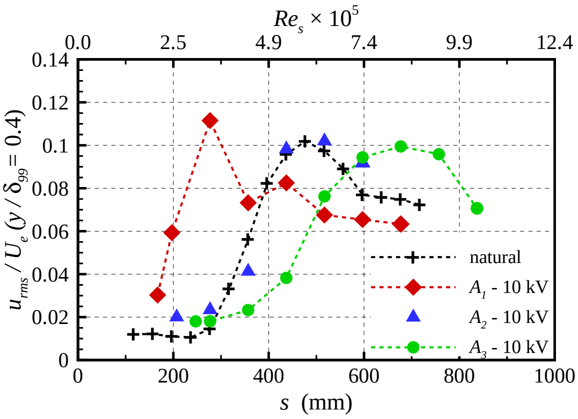

This higher level of u_{rms} / U_e in the laminar part is also present when the transition is delayed. The u_{rms} level is about 2% of the external velocity U_e, downstream actuator A_3, whereas it is close to 1% in the natural case. The boundary layer is excited when the plasma actuator is fired, which is similar to the measurements by Séraudie (2008) and Grundmann and Tropea (2009). Thus, it appears that if the boundary layer is excited by external perturbations (here, the ionic wind) of a particular level, depending on the action position, the transition onset can be delayed. If excitation of the boundary layer is too high, the transition is promoted. This is the case for actuator A_1. Otherwise, if the velocity fluctuation level is slightly increased by the ionic wind, the transition onset is delayed.

Figure 13 Power spectral density of velocity signals for actuator A_2 and natural flow, at a constant non-dimensional height (y / δ_{99} = 0.4) and s = 207 mm ($Re_s = 2.6 \times 10^5$) (see online version for colours)

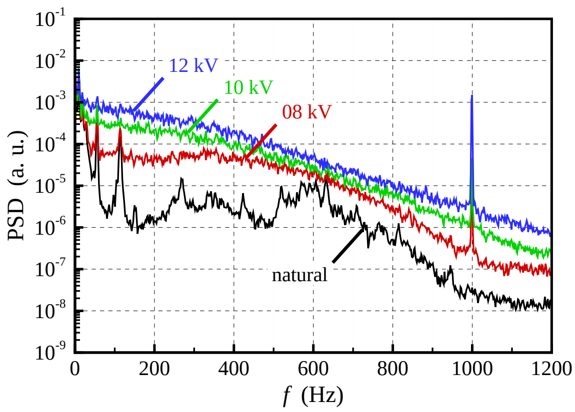

Downstream each actuator, the spectra show a higher level of energy than in the natural boundary layer, no matter what the effect on transition is (Figure 13, only for the actuator A_2). The mean level of velocity fluctuations is increased over a wide frequency range although the plasma actuator is fired at a frequency of f_{HV} = 1 kHz. The effect of a plasma actuator is to add momentum inside the boundary layer. Nevertheless a stabilising effect of the velocity profiles, leading to the delay of the transition onset, can be obtained depending on the ionic wind velocity. In this study, the free stream velocity is probably too high to observe this addition of momentum on the mean velocity profiles for the first measurement point downstream the plasma actuator. Indeed, the hot-wire probe has to be kept far enough to the actuator (i.e., the high voltage discharge) in order to avoid sparks. However, previous studies clearly reported this fact (e.g., Boucinha et al., 2008; Séraudie, 2008).

In order to determine what changes in the boundary layer under control, the instantaneous velocity signals are studied. A constant non-dimensional height of y / δ_{99} = 0.4 is considered, and velocity signals are plotted for a non-dimensional u_{rms} level of approximately 2% (Figure 14), 4% (Figure 15), and 8% (Figure 16). The level of u_{rms} / U_e for each case defines the s-position.

Figure 14 (a) Measurement points of velocity fluctuation distributions along the flat plate at a constant non-dimensional height (y / δ_{99} = 0.4) for the instantaneous velocity signals at a s-position where u_{rms} / U_e ~ 2% for (b) the natural case (s = 277 mm, $Re_s = 3.4 \times 10^5$), (c) a neutral case, actuator A_2 (10 kV, 1 kHz) at s = 207 mm ($Re_s = 2.6 \times 10^5$), and (d) a delay case, actuator A_3 (10 kV, 1 kHz) at s = 277 mm ($Re_s = 3.4 \times 10^5$) (see online version for colours)

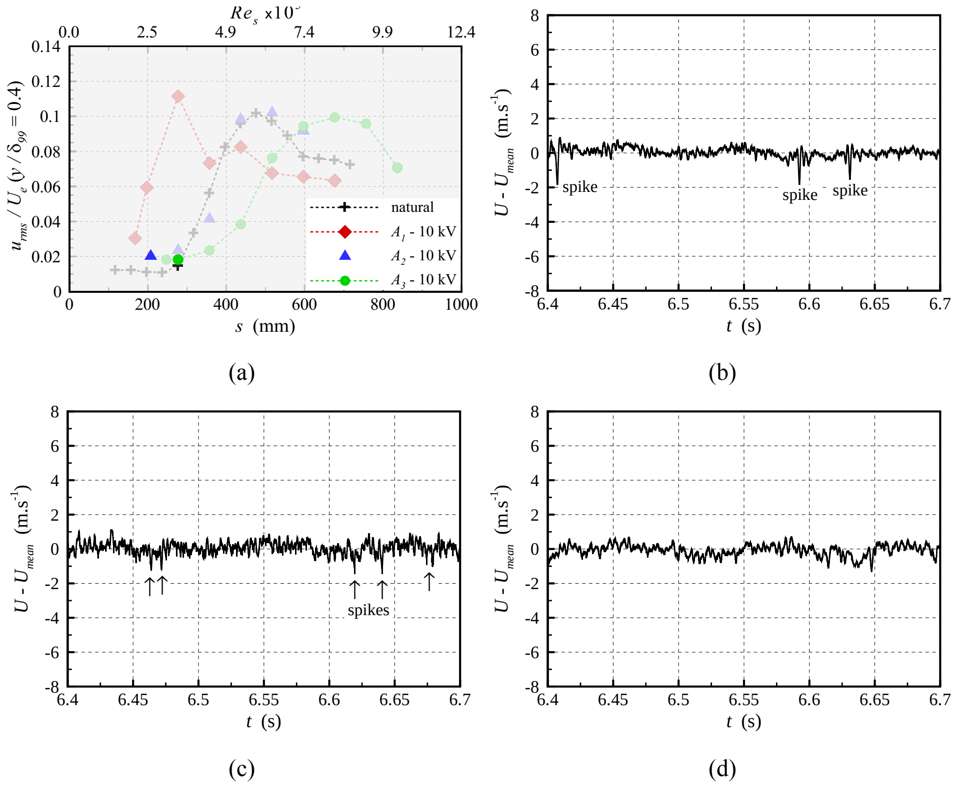

Just before the transition onset (u_{rms} / U_e ~ 2%), the natural and the neutral cases show that first spikes are present [Figures 14(b) and 14(c)]. They are not yet intense because the velocity drop remains quite weak. Their occurrence means the transition is going to begin shortly after. The signal for the neutral case is noisier because it shows the first measurement position downstream the actuator A_2 (due to the addition of momentum, not to electrical perturbations). For the delay case, a modification of the velocity signal is observed: it seems that the spikes do not yet appear [Figure 14(d)].

Figure 15 (a) Measurement points of velocity fluctuation distributions along the flat plate at a constant non-dimensional height ($y / \delta_{99} = 0.4$) for the instantaneous velocity signals at an s-position where $u_{rms} / U_e \sim 4\%$ for (b) the natural case ($s = 317$ mm, $Re_s = 3.9 \times 10^5$), (c) a neutral case, actuator A_2 (10 kV, 1 kHz) at $s = 357$ mm ($Re_s = 4.4 \times 10^5$), and (d) a delay case, actuator A_3 (10 kV, 1 kHz) at $s = 437$ mm ($Re_s = 5.4 \times 10^5$) (see online version for colours)

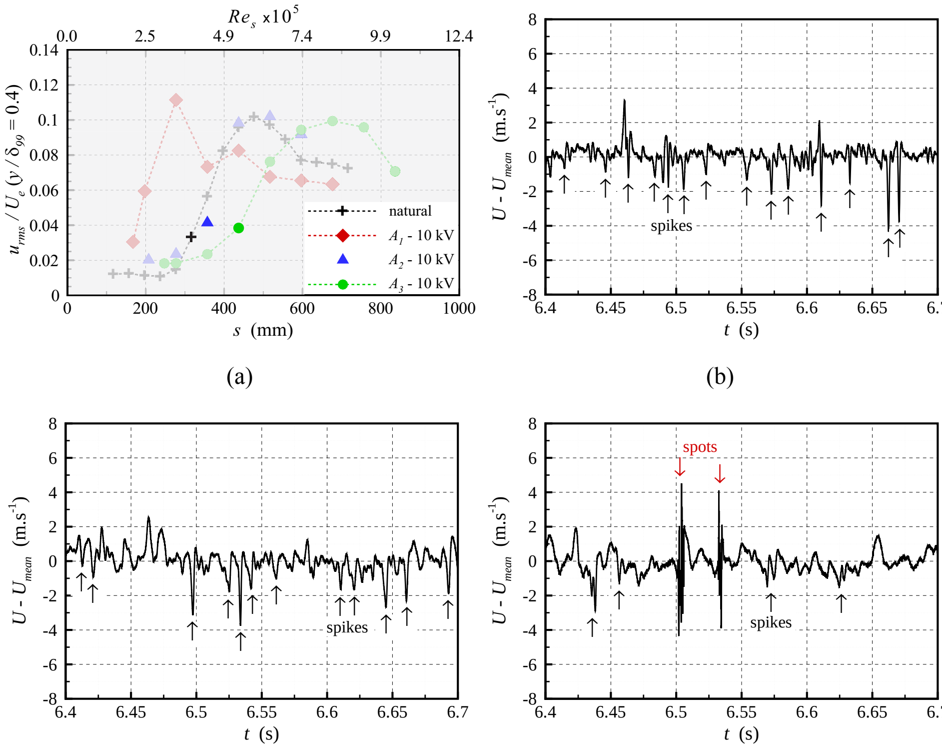

(a) (b)

(c) (d)

For the positions where $u_{rms} / U_e \sim 4\%$ the velocity signals show a transitional pattern. For the natural and delay cases, no important differences are observed [Figures 15(b) and 15(c)]. Spikes are more present and more intense than previously, leading to the increase of the u_{rms} level. For the delay case, a major difference is reported. Indeed, the first turbulent spots are present in the velocity signal besides spikes [Figure 15(d)]. In addition, the spike stage seems to be also modified: spikes are less numerous and less intense (i.e., the velocity drop is lower).

For the positions where $u_{rms} / U_e \sim 8\%$ the velocity signals show a fully transitional pattern. Spikes, turbulent spots and laminar parts are observed for the natural case [Figure 16(b)] and the delay case [Figure 16(c)]. As for the previous non-dimensional level of u_{rms}, the velocity signals exhibit differences. Spikes are more numerous in the neutral case, and seem more intense than in the delay case. Turbulent spots are present in both velocity signals. Thus, for a transition delay case, the modifications of the transition pathway by the plasma actuator can be observed from the beginning of the transition onset to the position where the boundary layer becomes fully turbulent. The plasma actuator does not modify only the location of the transition onset; it equally affects the transition process itself.

Figure 16 (a) Measurement points of velocity fluctuation distributions along the flat plate at a constant non-dimensional height (y / δ_{99} = 0.4) for the instantaneous velocity signals at an s-position where u_{rms} / U_e ~ 8% for (b) the natural case (s = 397 mm, $Re_s = 4.9 \times 10^5$), and (c) a delay case, actuator A_3 (10 kV, 1 kHz) at s = 517 mm ($Re_s = 6.4 \times 10^5$) (see online version for colours)

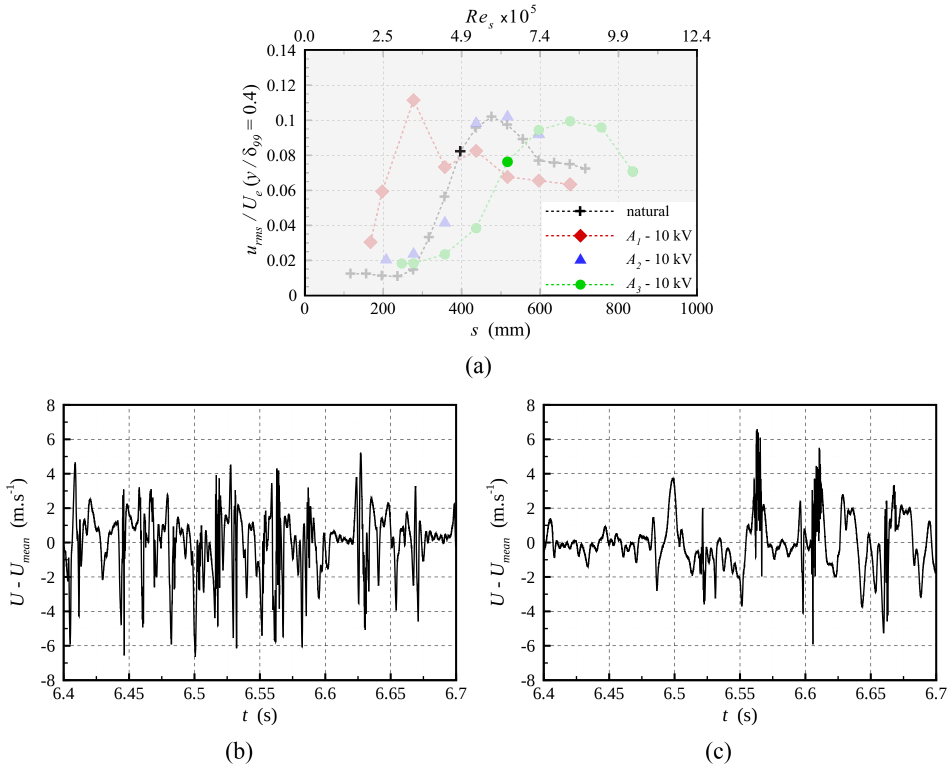

4.2 *Transition sensitivity to the actuator frequency*

The second way chosen to act on transition consisted in varying the actuator frequency f_{HV}. Previously, it has been shown that actuator A_2 is capable of inducing three effects on the transition. This actuator was therefore used to study the sensitivity of transition to the actuator frequency f_{HV}.

First, the voltage amplitude was set to V_{HV} = 12.7 kV in order to be sure that the ionic wind was high enough to delay the transition (Table 1). Two close frequencies were considered for f_{HV} (750 and 850 Hz). The maximum velocity of induced ionic wind was estimated at 4.4 m.s^{-1} and 4.6 m.s^{-1} respectively. So, the difference between these two velocities remains therefore weak, which means that the efficient parameter is mainly the actuator frequency. Velocity profiles were recorded for these two frequencies at a same s-position $s = 437$ mm (Figure 17). The non-manipulated boundary layer exhibits a mean velocity profile that does not fit with the Blasius profile: the boundary layer is transitional. This is confirmed with the u_{rms} level close to the wall that almost reaches its maximum value: 16% of U_e. When actuator A_2 is fired at 750 Hz, the mean velocity profile is closer to the Prandtl profile. The transition onset is promoted. At 850 Hz, the mean velocity profile matches with the Blasius profile, and the maximum u_{rms} level remains low (about 5% of U_e). Since the boundary layer transition is either promoted or delayed on the frequency band 750–850 Hz, a critical frequency seems exist around 800 Hz.

Figure 17 Mean (a) and fluctuation (b) velocity profiles at s-position $s = 437$ mm ($Re_s = 5.4 \times 10^5$) for actuator A_2, $V_{HV} = 12.7$ kV (see online version for colours)

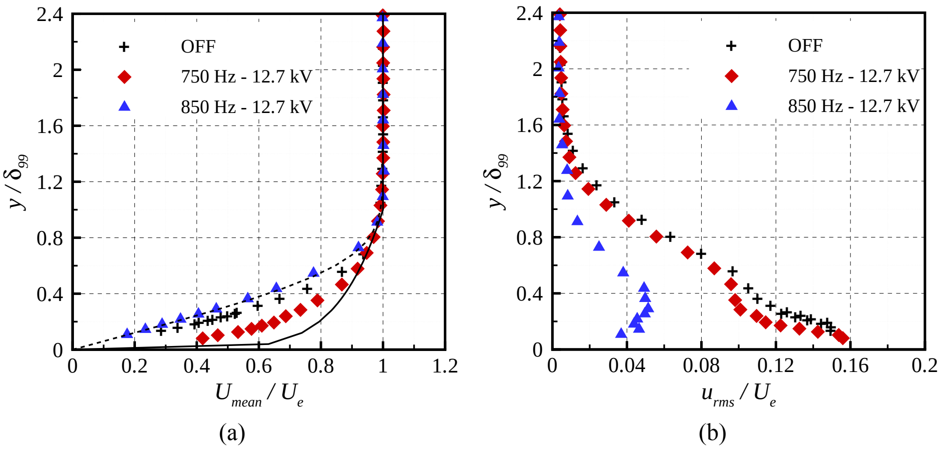

Note: Dashed line is Blasius profile, and solid line is Prandtl profile.

Figure 18 Variation of shape factor H_{12} for actuator A_2 with iso-ionic wind ($U_{act}^* = 3.3$ m.s^{-1}) at s-position $s = 437$ mm ($Re_s = 5.4 \times 10^5$) (see online version for colours)

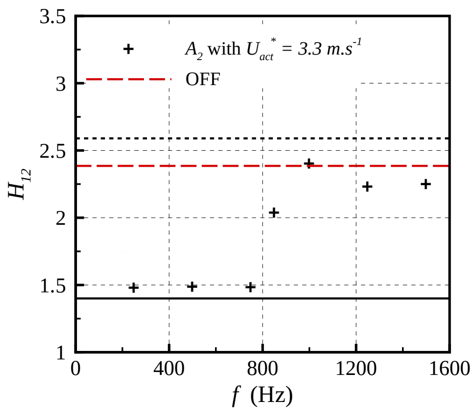

Note: Long-dashed line is the H_{12} value of natural flow, dashed line is the laminar value, $H_{12} = 2.59$, and solid line is the turbulent value, $H_{12} = 1.4$.

In order to confirm that a critical frequency exists, the maximum ionic wind velocity was maintained at a constant value of $U_{act}^{*} = 3.3$ m.s^{-1}, varying both voltage amplitude and frequency. Actuator A_2 was used, and f_{HV} ranged from 250 to 1,500 Hz, and respectively from 11.8 to 9.2 kV for V_{HV}. Variation in the shape factor H_{12} confirms that around 800 Hz, the boundary layer quickly passes from a laminar state to a turbulent one (Figure 18). Thus, to a given ionic wind velocity, which is high enough to induce an effect on the transition, it is the frequency by which the momentum is added inside the boundary layer that is important. This critical frequency could be related to the neutral frequency provided by the linear stability theory (Schlichting, 1979). According to this theory, the particular value of the critical frequency may vary, depending on several parameters such as the action position or the free stream velocity.

5 Conclusions

Experiments were performed in a wind tunnel on a flat plate geometry in order to test transition control by plasma actuators. The surface of the flat plate can be equipped with three surface DBD plasma actuators in the first part of the geometry, where the boundary layer is laminar. The free stream velocity was set at 20 m.s^{-1} in order to have the transition onset downstream the actuators, near the middle of the plate. The natural and manipulated boundary layers were mapped using a single hot-wire probe. By recording velocity profiles, the natural flow was characterised and the effects of the plasma actuators on the transition onset were highlighted. Two approaches were considered in order to act on the transition: a constant frequency of 1 kHz or the same ionic wind velocity. First, a parametric study was performed at the constant frequency in order to determine the influence of action position and voltage amplitude. Secondly, the frequency of the actuator was changed in order to highlight the sensitivity of transition to this parameter, with the ionic wind velocity maintained at a fixed value.

The parametric study, performed at a constant frequency, shows that the plasma actuator induces different effects on the transition onset position. By acting at a low amplitude voltage or far from the natural transition, its onset is promoted, whereas with a high amplitude voltage or close to the transition, its onset is delayed. Neutral cases were also observed. They correspond to the fact that the boundary layer development is not affected by the induced ionic wind. The mechanism by which the transition onset is modified seems due to an excitation of the boundary layer, since the u_{rms} levels are higher when the actuator is running, over a wide frequency range. In order to investigate the sensitivity of transition onset to the actuator frequency, a similar ionic wind velocity was produced. For actuator A_2, a critical frequency of 800 Hz was observed. Below this value, the transition onset is promoted, and delayed beyond. This observation could be in agreement with linear stability theory which predicts the existence of critical frequencies.

Finally, the plasma actuator can be used to add momentum inside the boundary layer in order to stabilise the velocity profiles and to act onto the natural instabilities. According to electrical parameters of the high voltage supplying the actuator, transition delay or promotion can be achieved. Moreover, in the transition delay case, a direct effect on the transition process itself is observable. The spike production stage is modified leading to an early appearance of the turbulent spots during the transition. Thus, it appears that the secondary instabilities could be also affected by using plasma actuators.

Acknowledgements

The authors would like to thank Stéphane Loyer (PRISME, University of Orléans) for his contribution to wind tunnel measurements, and Vincent Boucinha (formerly in PRISME, University of Orléans) for discussions and suggestions.

References

Arnal, D. and Juillen, J.C. (1978) 'Contribution expérimentale à l'étude de la réceptivité d'une couche limite laminaire, à la turbulence de l'écoulement général', *ONERA*, Rapport Tech. 1/5018 AYD.

Arnal, D., Juillen, J.C. and Michel, R. (1977) 'Analyse expérimentale et calcul de l'apparition et du développement de la transition de la couche limite', *AGARD Conference Proceedings*, AGARD-CP-224, 13-1.

Boucinha, V. (2009) 'Étude de l'écoulement induit par une décharge à barrière diélectrique surfacique – Contribution au contrôle des écoulements subsoniques par actionneurs plasmas', PhD thesis, University of Orléans, Orléans, France.

Boucinha, V., Joussot, R., Magnier, P., Leroy-Chesneau, A., Weber, R., Dong, B. and Hong, D. (2008) 'Characterization of the ionic wind induced by a Sine DBD actuator used for laminar-to-turbulent transition delay', *AIAA 4th Flow Control Conference*, 23–26 June, AIAA-2008-4210, Seattle, Washington.

Boucinha, V., Weber, R. and Kourta, A. (2011) 'Drag reduction of a 3D bluff body using plasma actuators', *International Journal of Aerodynamics*, Vol. 1, Nos. 3/4, pp.262–281.

Corke, T.C., Post, M.L. and Orlov, D.M. (2009) 'Single dielectric barrier discharge plasma enhanced aerodynamics: physics, modeling and applications', *Experiments in Fluids*, Vol. 46, No. 1, pp.1–26.

Duchmann, A., Reeh, A., Quadros, R., Kriegseis, J. and Tropea, C. (2009) 'Linear stability analysis for manipulated boundary-layer flows using plasma actuators', *Seventh IUTAM Symposium on Laminar-Turbulent Transition*, 23–26 June, Stockholm, Sweden.

Emmons, H.W. (1951) 'The laminar-turbulent transition in a boundary layer – Part I', *Journal of the Aeronautical Sciences*, Vol. 18, No. 7, pp.490–498.

Forte, M., Jolibois, J., Baudoin, F., Moreau, E., Touchard, G. and Cazalens, M. (2006) 'Optimization of a dielectric barrier discharge actuator and non-stationary measurements of the induced flow velocity-application to airflow control', *AIAA 3rd Flow Control Conference*, 5–8 June, AIAA-2006-2863, San Francisco, California.

Fransson, J., Talamelli, A., Brandt, L. and Cossu, C. (2006) 'Delaying transition to turbulence by a passive mechanism', *Physical Review Letters*, Vol. 96, No. 6, pp.064501-064501-4.

Grundmann, S. and Tropea, C. (2007) 'Experimental transition delay using glow-discharge plasma actuators', *Experiments in Fluids*, Vol. 42, No. 4, pp.653–657.

Grundmann, S. and Tropea, C. (2008) 'Active cancellation of artificially introduced Tollmien-Schlichting waves using plasma actuators', *Experiments in Fluids*, Vol. 44, No. 5, pp.795–806.

Grundmann, S. and Tropea, C. (2009) 'Experimental damping of boundary-layer oscillations using DBD plasma actuators', *International Journal of Heat and Fluid Flow*, Vol. 30, No. 3, pp.393–402.

Herbert, T. (1988) 'Secondary instability of boundary layers', *Annual Review of Fluid Mechanics*, Vol. 20, No. 1, pp.487–526.

Kachanov, Y.S. (1994) 'Physical mechanisms of laminar-boundary layer transition', *Annual Review of Fluid Mechanics*, Vol. 26, No. 1, pp.411–482.

Kendall, J.M. (1990) 'Boundary layer receptivity to freestream turbulence', *AIAA Fluid Dynamics, Plasma Dynamics and Lasers Conference*, 18–20 June, AIAA-1990-1504, Seattle, WA.

Klebanoff, P.S., Tidstrom, K.D. and Sargent, L.M. (1962) 'The three-dimensional nature of boundary layer instability', *Journal of Fluid Mechanics*, Vol. 12, No. 1, pp.1–34.

Laurentie, J.C., Jolibois, J. and Moreau, E. (2009) 'Surface dielectric barrier discharge: effect of encapsulation of the grounded electrode on the electromechanical characteristics of the plasma actuator', *Journal of Electrostatics*, Vol. 67, Nos. 2–3, pp.93–98.

Magnier, P., Boucinha, V., Dong, B., Weber, R., Leroy-Chesneau, A. and Hong, D. (2009) 'Experimental study of the flow induced by a sinusoidal dielectric barrier discharge actuator and its effects on a flat plate natural boundary layer', *Journal of Fluids Engineering*, Vol. 131, No. 1, pp.011203-011203-11.

Moreau, E. (2007) 'Airflow control by non-thermal plasma actuators', *Journal of Physics D: Applied Physics*, Vol. 40, No. 3, pp.605–636.

Örlü, R., Fransson, J. and Alfredsson, P. (2010) 'On near wall measurements of wall bounded-flow – the necessity of an accurate determination of the wall position', *Progress in Aerospace Sciences*, Vol. 46, No. 8, pp.353–387.

Porter, C., McLaughlin, T., Enloe, C.L., Font, G., Roney, J. and Baughn, J. (2007) 'Boundary layer control using a DBD plasma actuator', *AIAA 45th Aerospace Sciences Meeting and Exhibit*, 8–11 January, AIAA-2007-0786, Reno, Nevada.

Quadros, R.S. (2009) 'Numerical optimization of boundary-layer control using dielectric barrier discharge plasma actuators', PhD thesis, Technical University of Darmstadt, Darmstadt, Germany.

Saric, W.S., Reed, H.L. and Kerschen, E.J. (2002) 'Boundary-layer receptivity to freestream disturbances', *Annual Review of Fluid Mechanics*, Vol. 34, No. 1, pp.291–319.

Schlichting, H. (1979) *Boundary-layer Theory*, Mc Graw-Hill, New York.

Schubauer, G.B. and Klebanoff, P.S. (1956) 'Contributions on the mechanics of boundary-layer transition', NACA Technical Report No. 1289, pp.853–863.

Schubauer, G.B. and Skramstad, H.K. (1948) 'Laminar-boundary-layer oscillations and transition on a flat plate', NACA Technical Report No. 909, pp.327–357.

Séraudie, A. (2008) 'Implementation of plasma actuators on a flat plate: effect of ionic wind on laminar-turbulent transition', 10–12 March, *43rd AAAF colloque*, Poitiers, France.

Séraudie, A., Aubert, E., Naudé, N. and Cambronne, J.P. (2006) 'Effect of plasma actuators on a flat plate laminar boundary layer in subsonic conditions', *AIAA 3rd Flow Control Conference*, 5–8 June, AIAA-2006-3350, San Francisco, California.